J Mol Model (2013) 19:4897–4908
DOI 10.1007/s00894-013-1985-7

ORIGINAL PAPER

The intrinsic helical propensities of the helical fragments in prion protein under neutral and low pH conditions: a replica exchange molecular dynamics study

Xiaoliang Lu · Juan Zeng · Ya Gao · John Z. H. Zhang · Dawei Zhang · Ye Mei

Received: 8 April 2013 / Accepted: 22 August 2013 / Published online: 17 September 2013

Abstract Replica exchange molecular dynamics simulations in neutral and acidic aqueous solutions were employed to study the intrinsic helical propensities of three helices in both Syrian hamster (syPrP) and human (huPrP) prion proteins. The helical propensities of syPrP HA and huPrP HA are very high under both pH conditions, which implies that HA is barely involved in the helix-to-β transition. The SyPrP HB chain has a strong tendency to adopt an extended conformation, which is possibly involved in the mechanism of infectious prion diseases in Syrian hamster. HuPrP HC has more of a preference for the extended conformation than huPrP HA and huPrP HB do, which leads to the conjecture that it is more likely to be the source of β-rich structure for human prion protein. We also noticed that the presence of salt bridges is not correlated with helical propensity, indicating that salt bridges do not stabilize helices.

Keywords Prion · Helical propensity · pH condition · Replica exchange molecular dynamics

X. Lu · J. Zeng · Y. Gao · J. Z. H. Zhang · Y. Mei (✉)
Center for Laser and Computational Biophysics, State Key Laboratory of Precision Spectroscopy, Department of Physics and Institute of Theoretical and Computational Science, East China Normal University, Shanghai 200062, China
e-mail: ymei@phy.ecnu.edu.cn

J. Z. H. Zhang
Department of Chemistry, New York University, New York, NY 10003, USA

D. Zhang
Division of Chemistry and Biological Chemistry, School of Physical and Mathematical Sciences, Nanyang Technological University, Singapore 637371, Singapore

Introduction

Transmissible spongiform encephalopathies (TSE) [1] or prion diseases are a group of fatal neurodegenerative diseases that occur in many species (e.g., scrapie in sheep and chronic wasting disease in deer). On average, approximately one person in a million develops a prion disease per year [2], such as Creutzfeldt–Jakob disease (CJD) and Kuru [3, 4]. Recent studies have shown that prion susceptibility is species dependent. Syrian hamsters and mice are the species that are most susceptible to prion diseases, while rabbit, dog, and horse are the least likely to suffer this pathogenic process [5–13], although it is not impossible in those species [14]. The main pathogenetic mechanism for prion diseases is the misfolding of normal cellular prion protein (PrP^{c}) to the abnormal scrapie form (PrP^{Sc}) [1]. PrP^{Sc} has more β-sheet content and less α-helical content than PrP^{c} [15]. It can aggregate into amyloid fibrils through cross-β binding, which has been observed in X-ray scattering experiments [16]. Electron paramagnetic resonance and hydrogen/deuterium exchange experiments suggest that the C-terminal region of the prion protein may be involved in the core of amyloid fibrils formed from recombinant prion proteins (recPrP) [17, 18]. The human PrP 90–231 can form β-rich amyloid fibrils under acidic conditions [17, 19, 20], but this transition occurs very slowly in the absence of the denaturant [21].

Mature human prion protein is a glycoprotein comprising 209 amino acids (residues 23–231) that is attached to the membrane with glycosylphosphatidylinositol (GPI), which contains a flexible unstructured N-terminal domain (residue 23–124) and a C-terminal globular core (residues 125–228) consisting of three helices (HA: residues 144–156, HB: residues 174–194, HC: residues 200–228) and a short, two-stranded, antiparallel β-sheet (S1: residues 128–131, S2: residues 161–164) [22, 23]. The misfolding and aggregation of normal prion protein (PrP^{c}) into an infectious form (PrP^{Sc}) is

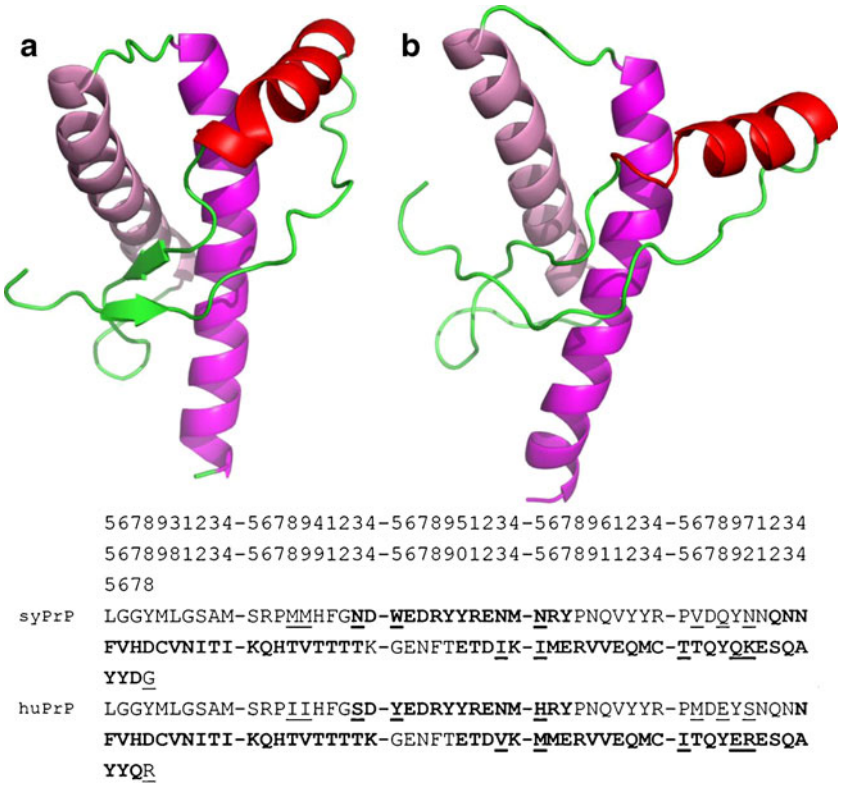

Fig. 1 Fitted free-energy landscapes of syPrP HA at 306 K under (*left*) neutral-pH and (*right*) low-pH conditions

the main event that occurs at the start of a prion disease [24]. Besides the differences in their conformations, PrP^{Sc} and PrP^{c} also have different biochemical properties. For instance, PrP^{c} is soluble, sensitive to proteinase K, and monomeric, while PrP^{Sc} forms insoluble amyloid and is resistant to proteinase K [1, 25, 26].

Although experiments are yet to elucidate the structure of PrP^{Sc} in atomic detail, it has been discovered that the β-rich PrP^{Sc} form accumulates into amyloid fibrils [15, 27–29]. These experimental observations have given rise to the hypothesis that the helices in PrP^{c} change into β-structures before polymerization into amyloid fibrils. Many studies have shown that the normal prion protein undergoes a temperature-induced, chemical-induced, three-state unfolding process in an acidic environment which leads to the formation of an intermediate state rich in β-structure [30, 31]. Various studies performed in vitro have indicated a relationship between low pH and misfolding/aggregation of prion protein [32]. In particular, a significant conformational change of human recPrP occurs under different pH conditions [30], and the spontaneous formation of fibrils of human recPrP has been observed at low pH [21].

All-atom molecular dynamics (MD) is potentially capable of providing data that can lead to a better understanding of the molecular mechanism for prion diseases, such as the conversion of the normal prion protein form (PrP^{c}) to the infectious scrapie isoform (PrP^{Sc}) [33–47]. Shamsir and Dalby [44] observed the formation of new β-sheets in the globular region of a D178N mutant, while Daggett and co-workers observed the elongation of the β-sheet and new β-structure formation in the N-terminal region at low pH [34, 48]. Recently, Miguel Machuqueiro and co-workers studied the reversibility of prion misfolding, and demonstrated that some conformational transitions induced by lowering the pH to 2 were reversible, by performing many constant-pH molecular dynamics simulations at neutral pH [49]. Circular dichroism (CD) and Fourier transform infrared spectroscopy studies indicated that the change in conformation from the normal cellular prion protein (PrP^{C}) to the pathogenic isoform (PrP^{Sc}) was marked by a loss of α-helix structure and a gain of β-content. Therefore,

Table 1 The population distributions (%) of Syrian hamster and human prion proteins

		syPrP			huPrP		
		α-Helix	β	ppII	α-Helix	β	ppII
HA	Neutral pH	53.0	10.0	5.0	48.5	14.8	6.4
	Low pH	44.5	14.0	9.6	54.2	9.0	7.8
HB	Neutral pH	34.8	19.4	13.8	40.5	13.2	10.5
	Low pH	39.0	15.0	14.0	45.6	12.0	10.0
HC	Neutral pH	46.4	12.0	7.7	39.7	14.8	8.8
	Low pH	44.2	13.2	10.6	40.4	15.4	12.6

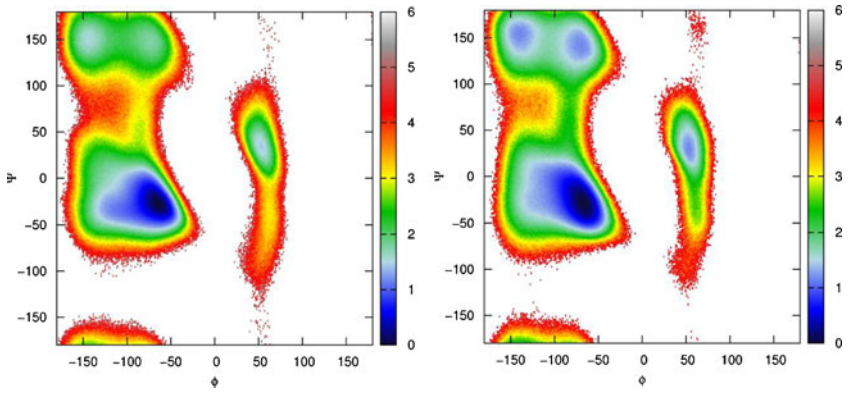

Fig. 2 Distance distributions of the salt bridges in syPrP HA at 306 K under (*left*) neutral-pH and (*right*) low-pH conditions

specific segments of PrP^C may undergo structural conversions, including HA, HB, and HC of the prion protein. HA of the prion protein has been investigated both experimentally and theoretically [50–52]. In the work described in the present paper, replica exchange molecular dynamics simulations [40] were utilized to investigate the secondary structural distributions of all three helices in human and Syrian hamster prion proteins under low and neutral pH conditions in aqueous solution. These different pH conditions lead to different protonation states of the residues Asp, His, and Glu, which are protonated at low pH and adopt their normal protonation states under neutral pH conditions. However, this work did not attempt to provide a thermodynamic explanation of the conversion from α-helix to β-sheet, because β-sheets in PrP^{Sc} are thought to be stabilized by cross-β interactions, such as hydrogen bonds and side-chain packing. Studying a single prion protein is not an effective way to address this interaction. Furthermore, metal-induced conformational changes were also not considered in this work; we only investigated the intrinsic helical propensities of the helices in PrP.

Methods

Simulation procedure

Replica exchange molecular dynamics (REMD) is now routinely applied to study protein folding and some other large-scale conformational changes [53, 54]. REMD is a generalized ensemble algorithm that performs a random walk in temperature space and helps the system to escape from local energy minima and explore conformational space more efficiently than conventional molecular dynamics (cMD). A set of simulations are performed at different target temperatures independently, and exchanges are attempted between adjacent replicas periodically according to the Metropolis criterion. The exchange probability is determined using [55]

$$P(1\leftrightarrow 2) = \min\left(1, \exp\left[\left(\frac{1}{K_B T_1} - \frac{1}{K_B T_2}\right)(U_1 - U_2)\right]\right),$$

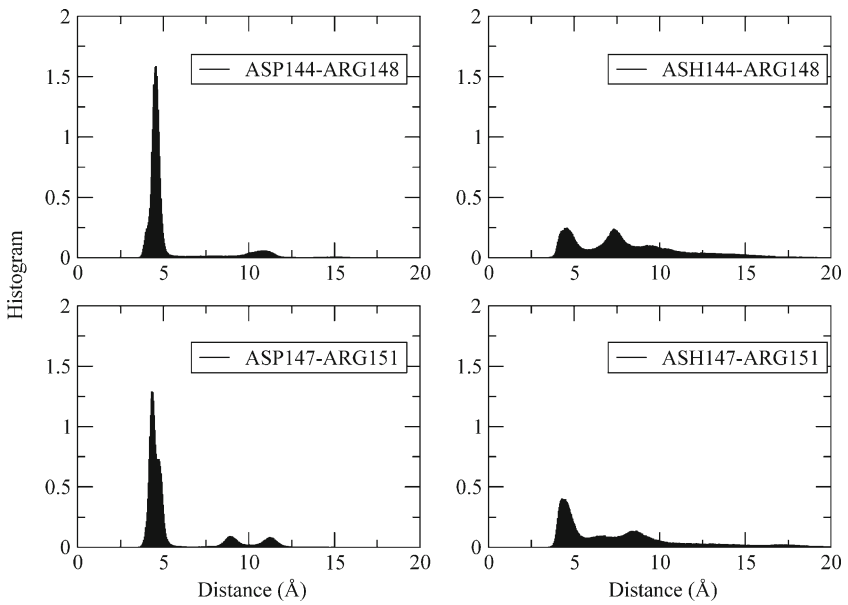

Fig. 3 Fitted free-energy landscapes of huPrP HA at 306 K under (*left*) neutral-pH and (*right*) low-pH conditions

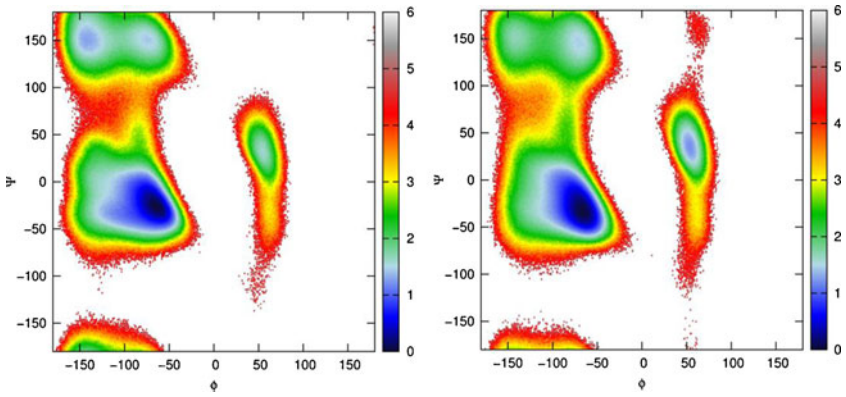

Fig. 4 Distance distributions of salt bridges in huPrP HA at 306 K under (*left*) neutral-pH and (*right*) low-pH conditions

where $P(1\leftrightarrow2)$ is the exchange probability, K_B is the Boltzmann constant, U_1 and U_2 are the instantaneous potential energies, and T_1 and T_2 are the reference temperatures. Altogether, 12 REMD simulations with 12 or 14 replicas were carried out for three helices (HA, HB, HC) in human prion protein (huPrP) and Syrian hamster prion protein (syPrP) under both neutral and low pH conditions. The temperatures were chosen as 266.0, 285.0, 306.0, 329.0, 353.0, 378.0, 405.0, 434.0, 464.0, 496.0, 530.0, and 565.00 K for the simulation of HA. In the simulation of HB, the temperatures were chosen as 270.0, 288.0, 307.0, 327.0, 349.0, 371.0, 395.0, 419.0, 445.0, 473.0, 502.0, and 532.0 K. For HC, the temperatures were set to 270.0, 285.0, 301.0, 318.0, 335.0, 353.0, 372.0, 392.0, 413.0, 434.0, 457.0, 481.0, 505.0, and 531.0 K. The starting structures were linear structures sealed by an acetyl group (CH_3CO–) at the N-terminus and an amine group (NH_2–) at the C-terminus. The peptides were relaxed until convergence was reached and then heated to the target temperatures in 200 ps. All replicas were equilibrated for 2 ns without exchanging temperatures and then underwent REMD simulations that continued for 160 ns for each replica. The AMBER99SB [56] force field and the generalized Born solvation model [57] were employed. The salt concentration was set to 0.2 M. All bonds with the hydrogen atoms were fixed using the SHAKE algorithm and the temperature was regulated by Langevin dynamics with a collision frequency of one per ps [58]. Nonbonded interactions were fully counted without any truncations. Swaps were attempted every 0.25 ps, and snapshots were saved at the same frequency. The AMBER 11 package was used for all of the REMD simulations and data analysis. Free energies along the chosen reaction coordinates were calculated using the weighted histogram analysis method (WHAM) [59, 60]. Main-chain dihedrals (φ,ψ) were classified into "α-helix" ($-100°<\varphi<-30°$ and $-67°<\psi<-7°$), "β" ($-180°<\varphi<-90°$ and $50°<\psi<240°$ or $160°<\varphi<180°$ and $110°<\psi<180°$), "ppII" ($-90°<\varphi<-20°$ and $50°<\psi<240°$), and other regions.

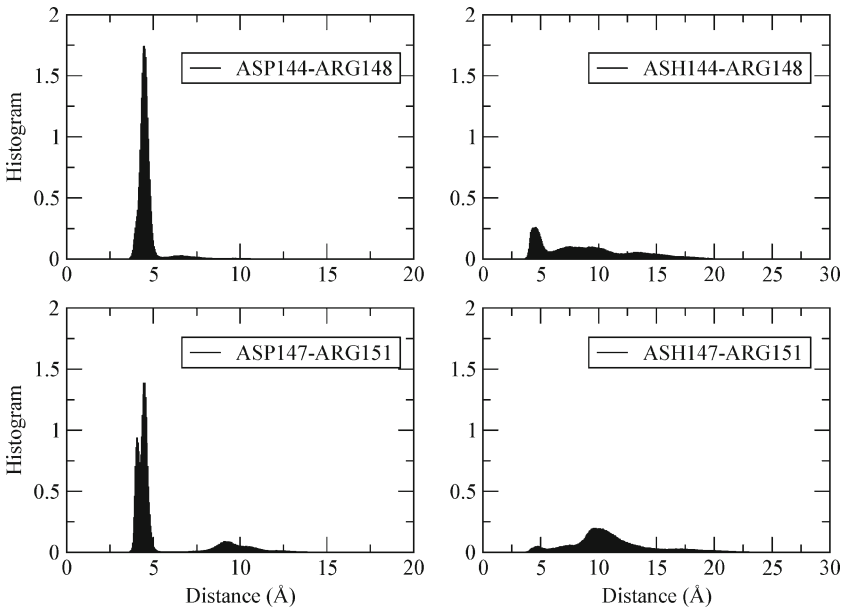

Fig. 5 Overall helical content populations for HA in (*left*) syPrP and (*right*) huPrP

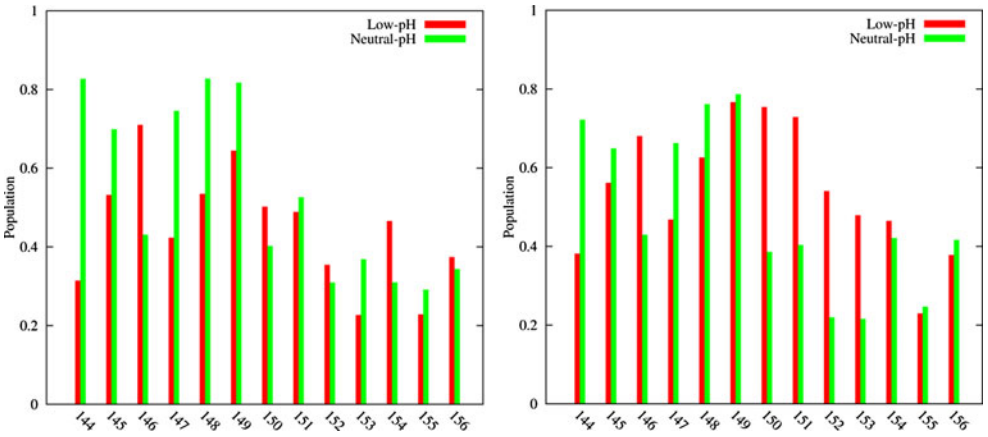

Fig. 6 *Top*: **a** NMR structure of syPrP 125–228 at pH 5.2 (PDB ID 1B10). **b** NMR structure of huPrP 125–228 at pH 7 (PDB ID 1HJM). The helices HA, HB and HC are colored *red*, *pink*, and *magenta*, respectively. *Bottom*: amino acid sequences (125–228) of syPrP and huPrP. HA, HB, and HC are shown in *boldface* successively. Differences in sequence are *underlined*

Results

Free-energy landscapes of syPrP HA and huPrp HA

The free energy of syPrP HA mapped to the main-chain dihedrals φ and ψ at 306 K is depicted in Fig. 1. This figure shows that the secondary structure mainly consists of α-helix, β, and ppII conformations, with the right-handed α-helix being the dominant conformation. Under neutral pH conditions, 7 of the residues each carry a charged side chain, and the total charge on syPrP HA is $-1e$. The global free-energy minimum resides in the right-handed α-helix domain, for which the free energy is about 1.5 kcal mol^{-1} lower than those of β, ppII, and the left-handed α-helix. The right-handed α-helix also covers a wider area (with free energy of <2.5 kca mol^{-1}) than the extended structure. The free energy of the barrier separating the extended conformations (β and ppII) and the right-handed α-helix domain is about 3 kcal mol^{-1} higher than that of the minimum. The population distributions for the major conformations are listed in Table 1. More than 50 % of the snapshots corresponded to the right-handed α-helix domain. The extended conformations (both β and ppII) were seen in only 15 % of the snapshots. Therefore, HA of syPrP has a strong tendency to form a right-handed α-helix under neutral pH conditions. When in the helical conformation, each pair of residues with oppositely charged side chains and sequences differing by 4 can form salt bridges. Figure 2 shows the distributions of the distances between the charged partners in the salt bridges. ASP144/ARG148 and ASP147/ARG151 show high probabilities of forming salt bridges. The distribution of the distance between GLU152 and ARG156 does not show a peak in the interacting region, but it does present a wide range (not shown). This observation indicates that the C-terminus of HA is less stable than the N-terminus. At low pH, two Asp and two Glu residues have their side chains protonated. The total charge strength is tripled, but the number of candidates for salt bridges is reduced. Lowering the pH reduces the right-handed α-helix population by about 8.5 % and increases the extended conformation population by 8.6 %. By studying the free-energy landscape, we noticed that the barrier separating the right-handed α-helical and ppII structures decreases correspondingly, which makes it easier to transit between right-handed α-helical and extended conformations. The free energy of the left-handed α-helix also drops, just like that of the extended conformations. The salt bridges that exist at neutral pH are disrupted (see the panel on the right in Fig. 2), with the distances covering a wider range.

In huPrP HA, three residues are different from their counterparts in syPrP HA. Two asparagine residues are replaced by one serine and one histidine, and a bulk tryptophan is replaced

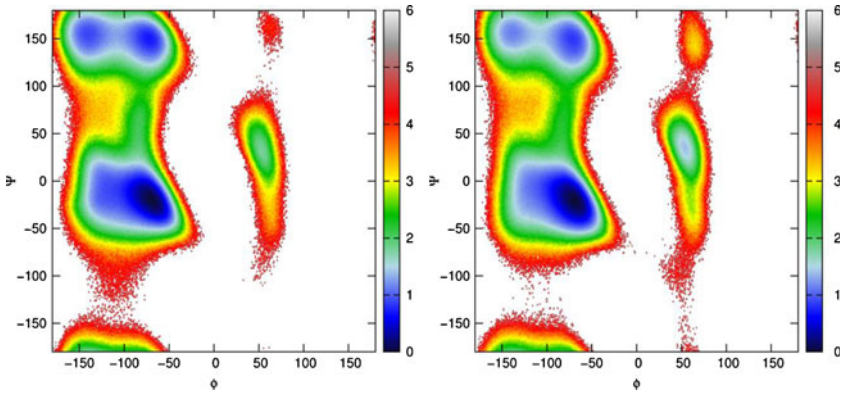

Fig. 7 Fitted free-energy landscapes of syPrP HB at 307 K under (*left*) neutral-pH and (*right*) low-pH conditions

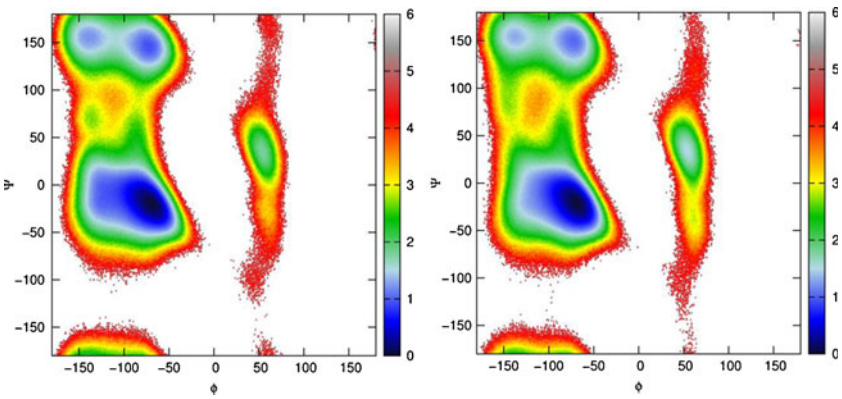

Fig. 8 Fitted free-energy landscapes of huPrP HB at 307 K under (*left*) neutral-pH and (*right*) low-pH conditions

by a tyrosine. The free-energy landscape of huPrP HA at neutral pH is quite similar to that of syPrP, with only marginal differences. The right-handed α-helix population is about 4.5 % lower than that of syPrP HA, while the populations of β and ppII are about 4.8 and 1.4 % higher. The barrier separating the right-handed α-helix and ppII domains (see Fig. 3) is even higher than that for syPrP HA. Under acidic conditions, the secondary structural distribution varies in the opposite manner to that of syPrP HA. The population of right-handed α-helices is increased by 5.7 %, while that of the extended conformation drops by 4.4 %. Similar to what is seen for syPrP HA, low pH lowers the barrier height between the right-handed α-helical and the extended conformations. The free energy in the left-handed α-helix domain decreases. Low pH has the same impact on the salt bridges as it does in syPrP HA. Under neutral conditions, salt bridges between ASP144 and ARG148 and between ASP147 and ARG151 show a prominent peaks in the strong-interaction region (see Fig. 4). However, both are eliminated at low pH. This observation indicates that the occurrence of salt bridges between residues separated by three residues is not correlated with helical preference, which goes against the viewpoint that salt bridges can help to stabilize helical conformations.

Helical propensity has a strong residue dependence, as shown in Fig. 5. Under neutral pH conditions, the N-terminal residues in syPrP HA have more of a tendency to adopt a helical conformation, while the population of helical conformations for the C-terminal residues is <40 %. Lowering the pH generally decreases the helical propensity, especially for N-terminal residues. The residue specificity of the helical population of huPrP HA under neutral pH conditions is similar to that of syPrP HA. However, lowering the pH increases the helical populations of residues TYR150 to MET154, which contrasts with what was observed for syPrP HA. Only ASP144 shows a significant decrease in its helical population. Arguably, salt bridges between residues i and $i+4$ help to stabilize helical conformations. In syPrP HA, three (ASP144, ASP147, and ARG148) out of the four residues involved in the salt bridges have reduced helical populations. However, ARG151 does not show much variation in its helical population with changes in pH. In huPrP HA, ASP144, ASP147, and ARG148 all show remarkable reductions in their helical populations, as also seen in syPrP HA. However, the helical population of ARG151 increases significantly. Therefore, the helical propensity does not show any correlation with the

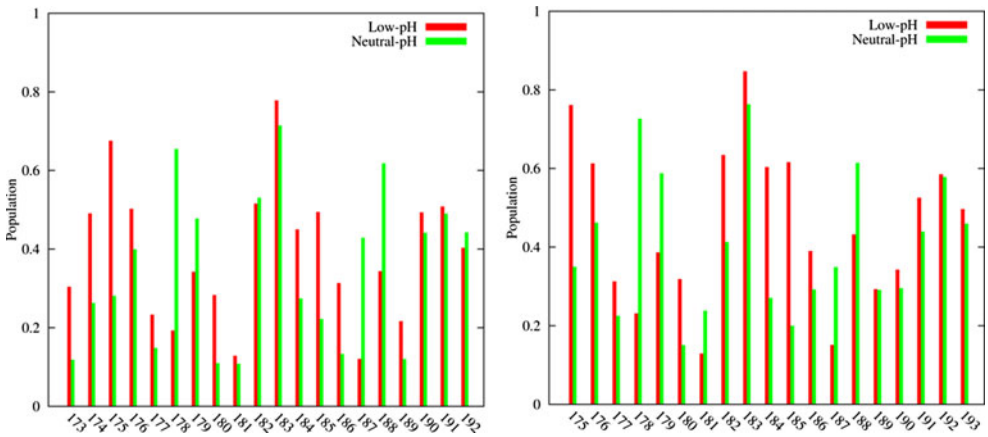

Fig. 9 Overall helical content populations for HB in (*left*) syPrP and (*right*) huPrP

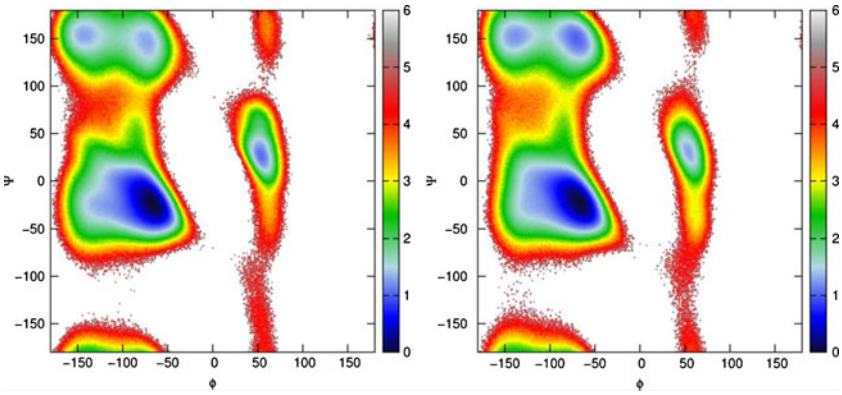

Fig. 10 Fitted free-energy landscapes of syPrP HC at 301 K under (*left*) neutral-pH and (*right*) low-pH conditions

occurrence of salt bridges. In other words, salt bridges do not stabilize helices.

Free-energy landscapes of syPrP HB and huPrP HB

Residues 171–199 in PrP are conserved in Syrian hamster and human, but the helical region shifts by 2 residues and is 1 residue shorter in huPrP (see Fig. 6). The free-energy landscapes of syPrP HB under neutral and low pH conditions are depicted in Fig. 7. Compared to syPrP HA, syPrP HB shows a large decrease in free energy for the extended conformations. The population in the right-handed α-helix domain is only 34.8 %, which is about 18 % lower than that for syPrP HA. The populations of β and ppII are each about 9 % larger. The barrier separating the right-handed α-helix and ppII domains is also lower. Therefore, conversion between a right-handed α-helix and extended conformations under neutral pH conditions is easier than it is for syPrP HA. Acidic conditions have the opposite effect on syPrP HB compared to syPrP HA. At low pH, the population of right-handed α-helices increases by 4.2 % and that of β decreases by 4.4 %. The barrier height between the right-handed α-helix domain and the ppII domain does not change too much.

The free-energy landscape of huPrP HB shown in Fig. 8 and the calculated helical propensities show only moderate differences from the free-energy landscape in Fig. 7, although the sequences of syPrP HB and huPrP HB differ by only three residues at the termini. The population in the right-handed α-helical domain is about 6 % higher in huPrP HB than it is in syPrP HB, but that of the β- conformation is about 6 % lower in huPrP HB. The barrier separating the right-handed α-helix domain and the ppII domain is a bit higher than that for syPrP HB. At low pH, the population of the right-handed α-helix is increased by 5 %. The populations of the β and ppII conformations show only tiny changes.

The residue-specific helical propensities shown in Fig. 9 indicate that protonation lowers the helical propensities of ASP178 and HIS187 in both syPrP and huPrP. The populations in the right-handed α-helical conformation of their neighbors on the right (CYS179 and THR188) also decrease at low pH, but the helical propensities of the N-terminal residues, as well as ILE184 and LYS185, increase at low pH.

Free-energy landscapes of syPrP HC and huPrP HC

HC is the longest chain among the three. The sequences of syPrP HC and huPrP HC differ by 5 residues. Low pH has a negligible impact on the helical propensity of syPrP HC. Upon moving from neutral to low pH, 4 % of the helical population shifts to extended conformations. This small perturbation of the populations makes almost no difference to the free-energy landscapes, as shown in Fig. 10. Only the salt bridge between ARG208 and GLU211 shows a sharp peak in the distance distribution at short distances; the distances for the other two

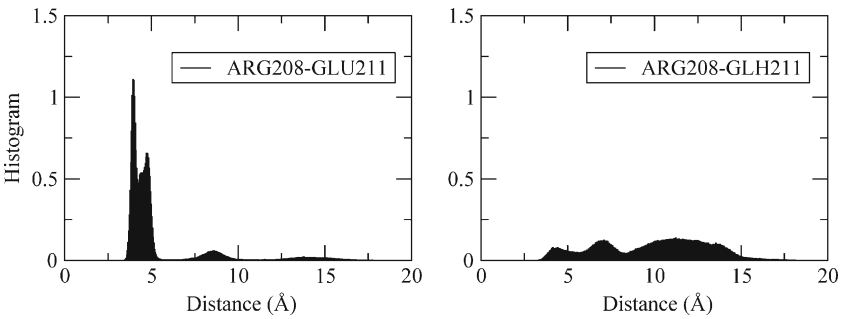

Fig. 11 Distance distributions of salt bridges in syPrP HC at 301 K under (*left*) neutral-pH and (*right*) low-pH conditions

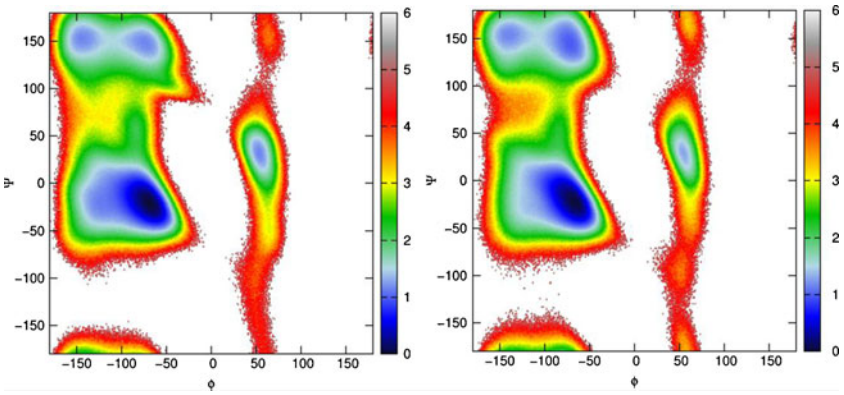

Fig. 12 Fitted free-energy landscapes of huPrP HC at 301 K under (*left*) neutral-pH and (*right*) low-pH conditions

(GLU200/LYS204 and LYS204/GLU207) are only rarely in the effective interaction zone (See Fig. 11). Low pH abolishes the strong interaction between the side chains of residues 208 and 211 and generates a flat distance distribution with a wide range. Under acidic conditions, the side chains of GLH200 and LYS204 prefer to be separated.

The impact of pH on the huPrP HC is also marginal. The right-handed α-helix, β, and ppII populations increase by 0.7, 0.6, and 3.8 %, respectively, upon lowering the pH. The increase in the population of major conformations is accompanied by a decrease in the occurrence of left-handed α-helices, which can be gauged from the diminished free-energy well in the left-handed α-helix domain shown in Fig. 12. The salt bridge between ARG208 and GLU211 is also abolished at low pH (see Fig. 13).

Although the overall helix contents in both syPrP HC and huPrP HC are not very sensitive to variations in pH, pH does have a strong effect on specific residues, and this residue-specific effect differs between syPrP HC and huPrP HC (see Fig. 14). For syPrP HC, at low pH, the helical propensities decrease for the residues in the first half and increase for residues 215 through 220. For huPrP HC, the helical propensities vary with the residue number in a more random manner. The helical propensities of the first 8 residues at the N-terminus increase with decreasing pH, whereas residues 209–212 and residues at the C-terminus prefer more extended conformations at low pH. Again, the helical propensity is not correlated with the occurrence of salt bridges. Although the helical contents of both ARG208 and GLU211 in syPrP decrease under acidic conditions, the helical propensity of ARG208 in huPrP increases a little bit.

Heat-induced melting of helices

The melting curves of all of these helices are shown in Fig. 15. Generally, the helix fractions decrease with increasing temperature, although some fragments show the opposite behavior at low temperatures. SyPrP HA is more stable at neutral pH than at low pH at all temperatures. HuPrP HA only shows higher stability at neutral pH than at low pH at high temperatures (>350 K). HB and HC in both syPrP and huPrP have almost the same helix fractions at both pH values, except that huPrP HB is less stable at neutral pH than under acidic conditions at low temperatures.

Principal component analysis of the correlated motion

Principal component analysis is capable of providing a clear picture of the overall motions of peptide chains of interest. As shown in Fig. 16, there are no strong correlations among the residues. At neutral pH, syPrP HA has more positive correlation among residues 146 to 150 but less positive correlation for residues 147 to 149 with the N-terminal than under acidic condition. This observation is also true for huPrP HA. For HB

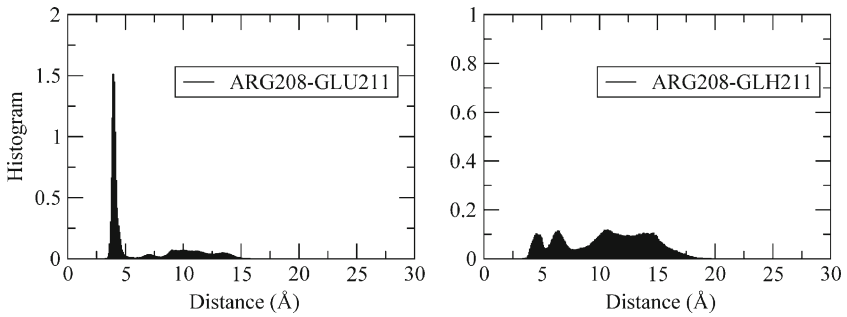

Fig. 13 Distance distributions of salt bridges in huPrP HC at 301 K under (*left*) neutral-pH and (*right*) low-pH conditions

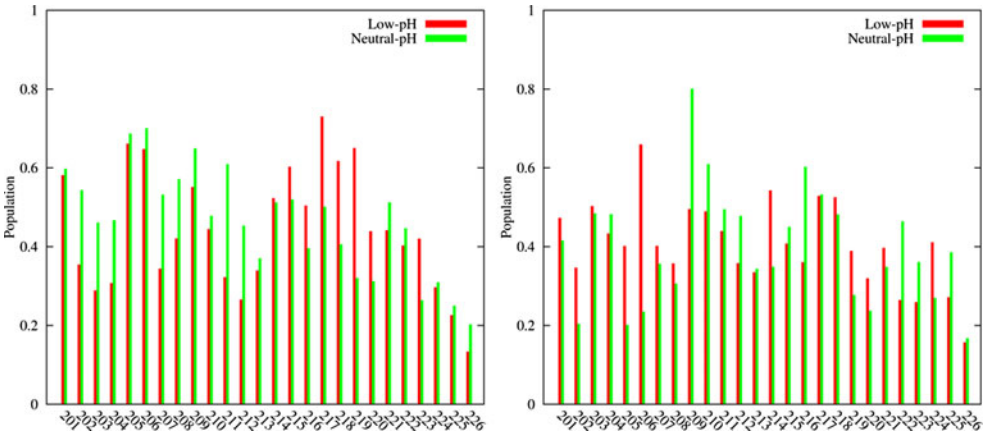

Fig. 14 Overall helical content populations for HC in (*left*) syPrP and (*right*) huPrP

and HC in both Syrian hamster and human, there are relatively strong correlations among the C-terminal residues, and these correlations are impervious to pH changes. For huPrP HB, decreasing the pH abolishes the weak correlations between the residues in the N-terminus and the C-terminus. Residues 205–209 in syPrP (huPrP) have positive (negative) correlations with residues 212–218 under acidic conditions, but this correlation is diminished under neutral pH conditions.

Discussion

Although Syrian hamster and human are both susceptible to prion diseases, their helical fragments respond differently to pH changes. The HA fragments in both species have a strong tendency to form a helix under neutral conditions. However, the helical propensity of HA shows opposite trends for Syrian hamster and human when the pH is changed from neutral to acidic: it increases in huPrP but decreases in syPrP. Nevertheless, the helix population of syPrP HA at low pH is still larger than those of syPrP HB and HC under the same conditions. Therefore, HA barely participates in the helix-to-β transition, especially for huPrP.

Under neutral pH conditions, over 33 % of the population of syPrP HB is in an extended conformation, which is the highest percentage among all the fragments at either pH. The transition barrier between helical conformations and ppII is also the lowest. Despite the increase in helical propensity at low pH, the population of the extended conformation is still higher than it is for other fragments. We conjecture that syPrP HB is likely involved in the mechanism of infectious prion diseases in Syrian hamster. The helix content in huPrP HB is about 5 % higher at low pH than it is at neutral pH. Low pH tends to protect this helical fragment. The population in the extended conformation is only weakly perturbed by applying

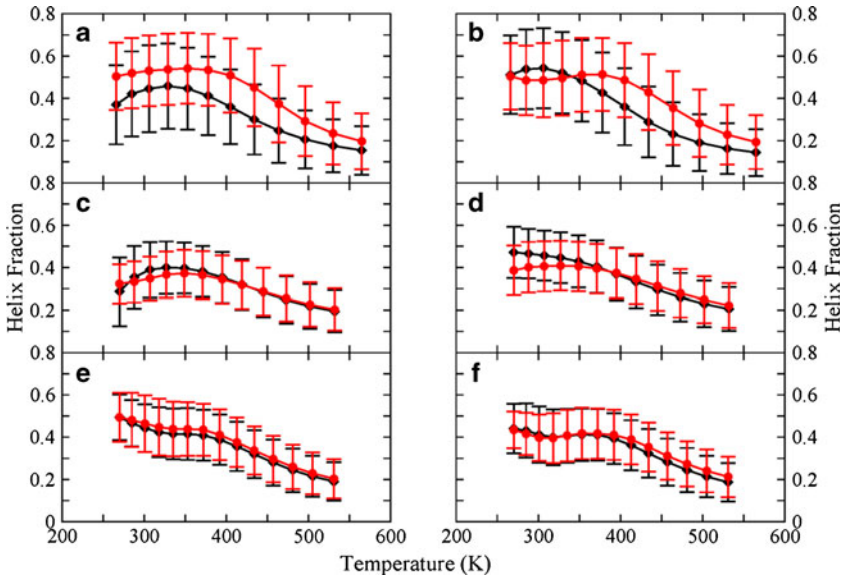

Fig. 15 Melting curves of **a** syPrP HA, **b** huPrP HA, **c** syPrP HB, **d** huPrP HB, **e** syPrP HC, and **f** huPrP HC under (*black*) low-pH and (*red*) neutral-pH conditions

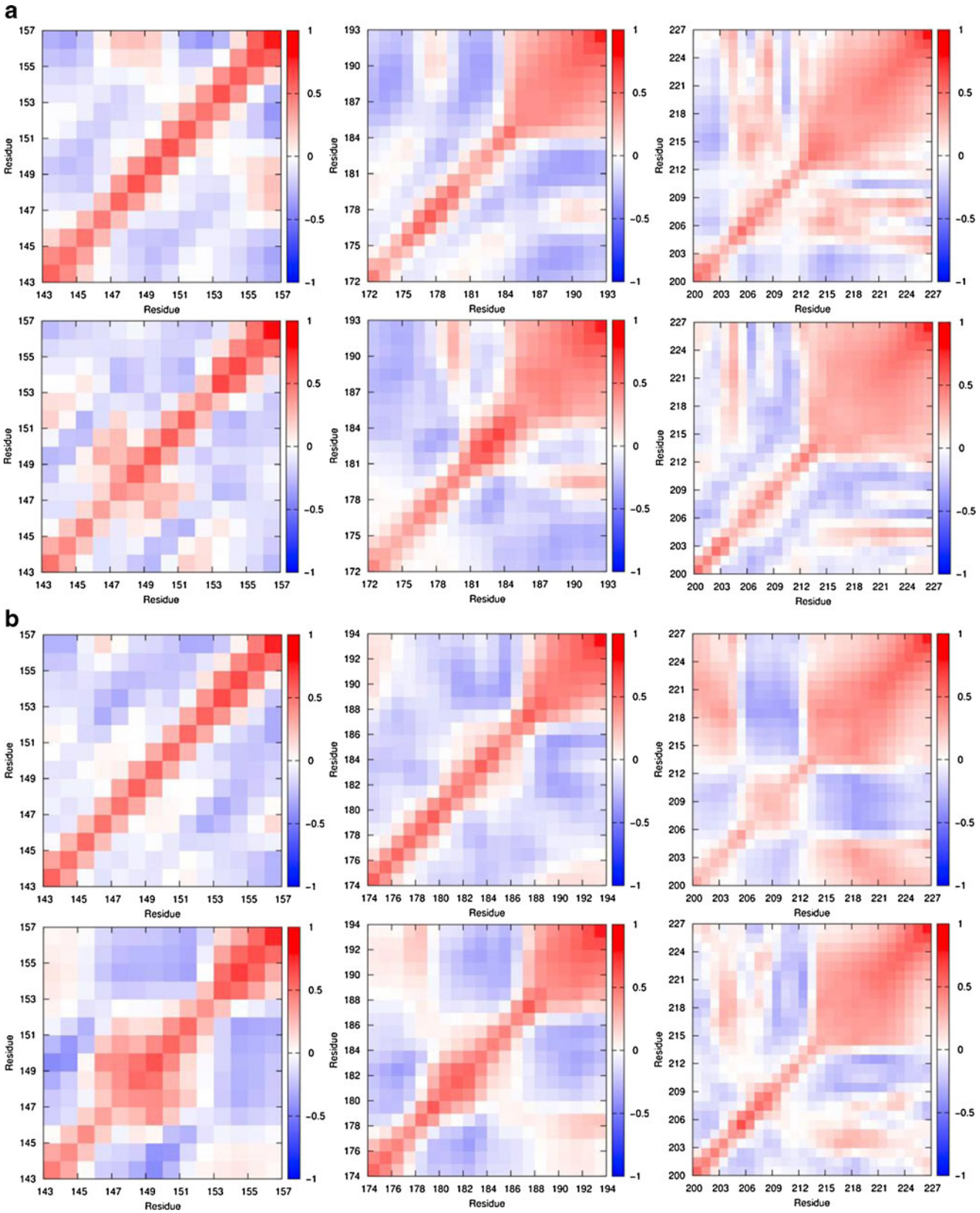

Fig. 16 Covariance matrices of C_α atoms for all of the chains considered in this study. A *red* point indicates that the two C_α atoms move in a correlated manner, while the *blue* (*darker*) color indicates that the atoms move in opposite directions. The *first column* shows data for HA, the *second column* for HB, and the *third column* for HC. The *first row* shows data for chains in Syrian hamster at pH4. the *second row* for chains in Syrian hamster at pH7, the *third row* for chains in human at pH4, and the *fourth row* for chains in human at pH7

a low pH, and this population is a little bit larger than that of huPrP HA.

The helical propensity of syPrP HC lies between those of syPrP HA and syPrP HB, and it is not very sensitive to pH variations. This also applies to huPrP HC. However, the population in the extended conformation for huPrP HC is larger than the corresponding populations for huPrP HA and huPrP HB. Therefore, huPrP HC is the most probable participant in the helix-to-β transition among all three helices in huPrP.

Conclusions

Replica exchange molecular dynamics simulations have been carried out to study the intrinsic helical propensities of three helical fragments in both the human prion protein and the Syrian hamster prion protein. Two pH conditions were considered, which were modeled by manually changing the protonation states of some titratable residues. Results for the residues show that a low pH decreases the helical propensity of syPrP HA but increases that of huPrP HA. Since Syrian hamster and human are both susceptible to infectious prion diseases, we assert that huPrP HA is not responsible for the α-to-β conversion. This observation is consistent with the work of Jan Ziegler and co-worker, who found that HA retained a high level of helicity under a wide range of conditions, such as high salt, pH variation, and the presence of organic co-solvents [61]. The HB fragment in syPrP has a strong tendency to form extended structures at both neutral and low pH, which leads us to conjecture that it is involved in the mechanism of infectious prion diseases in Syrian hamster. Acidic conditions increase the helix content of huPrP HB by around 5 %, while the HC chain in huPrP is insensitive to pH variation. We thus infer that HC is more likely to be involved in β-rich structures in human. During the preparation of this paper, Chen and Thirumalai studied the unfolding of human PrP^{C}, and they showed that HB and HC are the initiation sites for the PrP^{C} to PrP^{SC} transitions [62]. We also noticed that the occurrence of salt bridges is not correlated with the helical propensity, indicating that salt bridges do not stabilize helices.

Acknowledgments We are grateful for the financial support from the National Natural Science Foundation of China (grant nos. 10974054, 20933002, and 21173082). We also thank Prof. Donghai Lin and Dr. Yi Wen at Xiamen University for helpful discussions. The High Performance Computer Center of East China Normal University is acknowledged for its support in allowing us CPU time.

References

1. Prusiner SB (1998) Proc Natl Acad Sci USA 95:13363
2. Caughey B (2003) Br Med Bull 66:109
3. Mastrianni JA (2004) Clin Neurosci Res 3:469
4. Millhauser GL (2007) Copper and the prion protein: methods, structures, function, and disease. In: Annual review of physical chemistry, vol 58. Annual Reviews, Palo Alto, p 299
5. Khan MQ, Sweeting B, Mulligan VK, Arslan PE, Cashman NR, Pai EF, Chakrabartty A (2010) Proc Natl Acad Sci USA 107:19808
6. Gibbs CJ Jr, Gajdusek DC (1973) Science 182:67
7. Thomzig A, Cardone F, Kruger D, Pocchiari M, Brown P, Beekes M (2006) J Gen Virol 87:251
8. Kimberlin RH, Walker C (1977) J Gen Virol 34:295
9. Bessen RA, Marsh RF (1992) J Gen Virol 73(Pt 2):329
10. Lasmezas CI, Deslys JP, Robain O, Jaegly A, Beringue V, Peyrin JM, Fournier JG, Hauw JJ, Rossier J, Dormont D (1997) Science 275:402
11. Chandler RL (1961) Lancet 1:1378
12. Hill AF, Joiner S, Linehan J, Desbruslais M, Lantos PL, Collinge J (2000) Proc Natl Acad Sci USA 97:10248
13. Barlow RM, Rennie JC (1976) Res Vet Sci 21:110
14. Chianini F, Fernández-Borges N, Vidal E, Gibbard L, Pintado B, de Castro J, Priola SA, Hamilton S, Eaton SL, Finlayson J, Pang Y, Steele P, Reid HW, Dagleish MP, Castilla J (2012) Proc Natl Acad Sci USA 109:5080
15. Pan KM, Baldwin M, Nguyen J, Gasset M, Serban A, Groth D, Mehlhorn I, Huang Z, Fletterick RJ, Cohen FE (1993) Proc Natl Acad Sci USA 90:10962
16. Sunde M, Serpell LC, Bartlam M, Fraser PE, Pepys MB, Blake CCF (1997) J Mol Biol 273:729
17. Cobb NJ, Sonnichsen FD, McHaourab H, Surewicz WK (2007) Proc Natl Acad Sci USA 104:18946
18. Lu XJ, Wintrode PL, Surewicz WK (2007) Proc Natl Acad Sci USA 104:1510
19. Swietnicki W, Morillas M, Chen SG, Gambetti P, Surewicz WK (2000) Biochemistry 39:424
20. Morillas M, Vanik DL, Surewicz WK (2001) Biochemistry 40:6982
21. Cobb NJ, Apetri AC, Surewicz WK (2008) J Biol Chem 283:34704
22. Wuthrich K, Riek R (2001) Adv Protein Chem 57:55
23. Harris DA (1999) Clin Microbiol Rev 12:429
24. Prusiner SB, McKinley MP, Bowman KA, Bolton DC, Bendheim PE, Groth DF, Glenner GG (1983) Cell 35:349
25. Abid K, Soto C (2006) Cell Mol Life Sci 63:2342
26. Cobb NJ, Surewicz WK (2009) Biochemistry 48:2574
27. Nguyen JT, Inouye H, Baldwin MA, Fletterick RJ, Cohen FE, Prusiner SB, Kirschner DA (1995) J Mol Biol 252:412
28. Jackson GS, Hill SF, Joseph C, Hosszu L, Power A, Waltho JP, Clarke AR, Collinge J (1999) Biochim Biophys Acta Protein Struct Mol Enzymol 1431:1
29. Caughey BW, Dong A, Bhat KS, Ernst D, Hayes SF, Caughey WS (1991) Biochemistry 30:7672
30. Swietnicki W, Petersen R, Gambetti P, Surewicz WK (1997) J Biol Chem 272:27517
31. Hornemann S, Glockshuber R (1998) Proc Natl Acad Sci USA 95:6010
32. DeMarco ML, Daggett VCR (2005) Biol 328:847
33. DeMarco ML, Silveira J, Caughey B, Daggett V (2006) Biochemistry 45:15573
34. DeMarco ML, Daggett V (2004) Proc Natl Acad Sci USA 101:2293
35. Ding F, LaRocque JJ, Dokholyan NV (2005) J Biol Chem 280:40235
36. Dima RI, Thirumalai D (2004) Proc Natl Acad Sci USA 101:15335
37. Langella E, Improta R, Barone V (2004) Biophys J 87:3623
38. De Simone A, Dodson GG, Verma CS, Zagari A, Fraternali F (2005) Proc Natl Acad Sci USA 102:7535
39. De Simone A, Zagari A, Derreumaux P (2007) Biophys J 93:1284
40. Langella E, Improta R, Crescenzi O, Barone V (2006) Proteins 64:167
41. Gu W, Wang TT, Zhu J, Shi YY, Liu HY (2003) Biophys Chem 104:79
42. Barducci A, Chelli R, Procacci P, Schettino V (2005) Biophys J 88:1334
43. Sekijima M, Motono C, Yamasaki S, Kaneko K, Akiyama Y (2003) Biophys J 85:1176

44. Shamsir MS, Dalby AR (2005) Proteins 59:275
45. Shamsir MS, Dalby AR (2007) Biophys J 92:2080
46. van der Kamp MW, Daggett V (2010) Biophys J 99:2289
47. Campos SRR, Machuqueiro M, Baptista AM (2010) J Phys Chem B 114:12692
48. Alonso DOV, DeArmond SJ, Cohen FE, Daggett V (2001) Proc Natl Acad Sci USA 98:2985
49. Vila-Vicosa D, Campos SRR, Baptista AM, Machuqueiro M (2012) J Phys Chem B 116:8812
50. Hornemann S, Korth C, Oesch B, Riek R, Wider G, Wuthrich K, Glockshuber R (1997) FEBS Lett 413:277
51. Norstrom EM, Mastrianni JA (2006) J Virol 80:8521
52. Wille H, Michelitsch MD, Guenebaut V, Supattapone S, Serban A, Cohen FE, Agard DA, Prusiner SB (2002) Proc Natl Acad Sci USA 99:3563
53. Hansmann UHE, Okamoto Y (1999) Curr Opin Struct Biol 9:177
54. Mitsutake A, Sugita Y, Okamoto Y (2001) Biopolymers 60:96
55. Sugita Y, Okamoto Y (1999) Chem Phys Lett 314:141
56. Hornak V, Abel R, Okur A, Strockbine B, Roitberg A, Simmerling C (2006) Proteins 65:712
57. Onufriev A, Bashford D, Case DA (2004) Proteins 55:383
58. Ryckaert JP, Ciccotti G, Berendsen HJC (1977) J Comput Phys 23: 327
59. Kumar S, Bouzida D, Swendsen RH, Kollman PA, Rosenberg JM (1992) J Comput Chem 13:1011
60. Chodera JD, Swope WC, Pitera JW, Seok C, Dill KA (2007) J Chem Theory Comput 3:26
61. Ziegler J, Sticht H, Marx UC, Muller W, Rosch P, Schwarzinger S (2003) J Biol Chem 278:50175
62. Chen J, Thirumalai D (2012) Biochemistry 52:310